Experimental Study of a Gas Bubble Passing Through a Liquid-Liquid Interface in a Thin Gap Column

BSc Thesis

Delft University of Technology
Faculty of Applied Sciences
Department of Chemical Engineering

Starting date: 14th of February 2018
Defense date: 16th of July 2018

Author:
Lorenzo Presilli
Student number: 4462807

Supervisor:
L. Portela

Reviewers:
Dr. L. Portela
Dr. Ir. D. Vermaas
Ir. M. Mandalahalli

Abstract

This study aims to get a better understanding of the passing phenomena of a rising gas bubble passing through a liquid-liquid interface. This is done experimentally with a narrow column by capturing the rising gas bubble with high speed imaging. The light phase consists of silicone oil and the heavy phase consists of water with different glycerine concentrations. The viscosity ratio of the liquids and the size of the bubbles were varied in the experiments. Experimental results show the effect of liquid viscosity and bubble size, represented as the Reynolds number, on the retention time at the interface. Moreover results show the shape of the bubble when moving through the phases and compares the experimental results with bubbles in infinite medium. The results also gave interesting insights into conditions where the bubble passing the interface was encapsulated by heavy liquid.

Contents

1 Introduction **3**
1.1 Motivation . . . 3
1.2 Theory . . . 4

2 Materials and Methods **7**
2.1 Experimental setup . . . 7
2.2 Bubble volume . . . 9
2.3 Refractive index . . . 9
2.4 Image processing . . . 10
2.5 Data processing . . . 12

3 Results and Discussion **15**
3.1 Retention time at the interface . . . 15
3.2 Entrainment of heavy liquid . . . 17
3.3 Shape of the bubble . . . 20

4 Conclusion and recommendation **23**
4.1 Conclusion . . . 23
4.2 Recommendation . . . 23

Bibliography **25**

A Appendix **27**
A.1 Height plots . . . 27
A.2 Tables . . . 30
A.3 Experimental procedure . . . 32
A.4 Cleaning procedure . . . 32

Chapter 1

Introduction

1.1 Motivation

Bubble flows are present in many industrial applications. In steel refining processes molten steel and slag react. To enhance the contact area between the two phases gas is injected that passes through both phases and causes entrainment of the heavy phase into the light phase (Song et al., 2017). Another example are gas-liquid-liquid direct-contact evaporators that concentrate solutions by bubbling superheated gas (Ribeiro Jr, 2005). Many more applications for bubble flows exist (Shimizu et al., 2000).

When an interface is present in the system bubbles will show certain passing phenomena, as is the case in the steel refining processes where there is entrainment of heavy liquid into the light phase whereas in other cases there is no entrainment. How long a bubble is retained by the interface also varies across different conditions. In 2007 Kemiha et. al. researched this retention time experimentally by varying bubble diameter and found that by reducing bubble diameter, retention time increased(Kemiha et al., 2007). In 2015 Singh studied the effect of many parameters such as density difference, viscosity difference and bubble diameter on among other things the retention time and retention height (Sing and Bart, 2015). This was done numerically which has the advantage that all parameters can be kept constant except for the parameter that is studied.

When studying rising bubbles that pass through an interface, all the passing phenomena depend on the system's parameters and the forces involved. An important force is the driving force of the bubble, which is the buoyancy force. Then there is the interface which produces a certain surface tension force. Properties of the phases the bubble is rising through also influence the passing phenomena, such as liquids density an viscosity that will influence terminal velocity. In Figure 1.1 the bubble can be seen at different stages when rising through the liquids. The bubble is rising through the bottom liquid (1.1a) and when reaching the interface, some liquid is stuck in between the interface and the bubble which is referred to as the heavy liquid film (1.1b). This liquid needs to be squeezed by the bubble and the interface before the bubble passes the interface (1.1c). This drainage thus depends on buoyancy force, surface tension force and liquid properties.

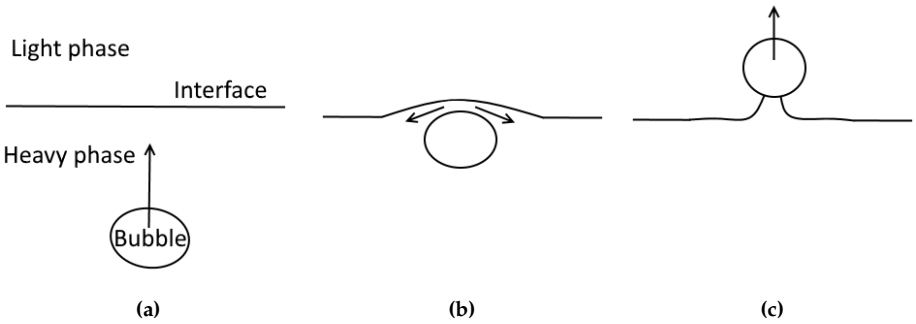

Figure 1.1: In this Figure the bubble can be seen rising(1.1a), draining the heavy liquid film(1.1b) and eventually passing the interface(1.1c).

This study will try to gain qualitative and quantitative insights on the passing phenomena of a bubble at a liquid-liquid interface. To achieve this, a narrow column is used in order to reduce bubble oscillation and obtain focused images of the bubble. Bubble size will be varied to study the phenomena at different body forces. The viscosity ratio of the liquids will be varied by using different concentrations of glycerine in the bottom liquid and by using silicone oil, which has a wide range of viscosity, as top liquid. The main goal is to study specifically the retention time of the bubble at the interface, the entrainment of heavy liquid and the shape of the bubble.

1.2 Theory

1.2.1 Bubble formation

Understanding bubble formation is important since bubble size is one of the parameters that is changed in the experiments. Bubble formation depends on many factors (Snabre and Magnifotcham, 1998): surface tension between water and air (F_s), buoyancy force produced by pressure gradient (F_b), inertial force due to expansion (F_i), drag force (F_D) and momentum created by the added mass (F_m). These forces can be seen in Figure 1.2. All these factors contribute to the final bubble size and thus finding a model for non steady state bubble formation becomes complicated. In a simplified situation in which flow rate is low enough so that F_i, F_m and F_D are relatively small compared to F_s and F_b. The formation of the bubble becomes steady state. During experiments it is important to avoid pressure drop in the gas chamber in order to produce bubbles of the same size and thus a mass flow pomp is used since this prevents pressure drop. One purpose is to produce bubbles of the same size across the different viscous liquids. There are still some differences in density and surface tension between the different bottom liquids and thus bubble size also has some variation. For example to indicate the effect of bottom liquid on bubble size, with an orifice with inner diameter 1.016 mm in water and glycerine 92% bubbles were produces with average equivalent diameters of 3.08 and 2.75 mm respectively.

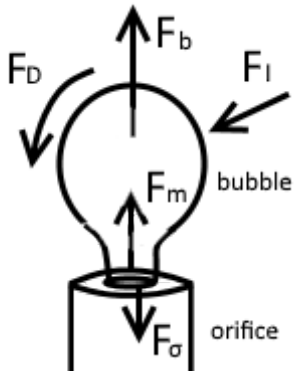

Figure 1.2: Schematic of the formation of a gas bubble and the forces involved.

1.2.2 Rising of the bubble

When the bubble detaches from the orifice, it will rise through the liquid. The rising of the bubble is driven by the buoyancy force which can be seen in equation 1.1. The buoyancy force is driven by density difference between the air in the bubble and the liquid surrounding it. However the liquid needs to flow around the bubble and causes resistance in the form of the drag force which can be seen in equation 1.2, which is among other things dependent on the bubbles speed. The bubble is thus accelerating when detached from the orifice but as the bubble reaches higher speeds, the drag forces increase. This will eventually lead to a balance between drag force and buoyancy force, causing the bubble to have a terminal velocity (van den Akker and Mudde, 1996). In Figure 1.3 the forces acting on the bubble can be seen.

$$\mathrm{F}_b = \delta \rho V g \tag{1.1}$$

$$\mathrm{F}_D = 0.5 \rho u^2 C_D A \tag{1.2}$$

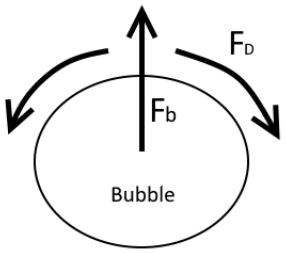

Figure 1.3: Bubble rising through a liquid, including the working forces.

1.2.3 Shape of the bubble

When a bubble rises through a liquid, it can take many shapes ranging from spherical to ellipsoidal to spherical-cap (Clift et al., 1978). Bubbles deform due to shear stress, caused by the drag force. The interface of the bubble tries to minimize its surface area because the gas molecules and water molecules dislike each other and thus a larger surface area is thermodynamically unfavourable, there is a force perpendicular at the surface of the bubble caused by the different attraction between molecules which is called the surface tension force as can be seen in equation 1.3. A bubble will eventually find a balance between forces created by surface tension and forces created by shear stress, resulting in a specific shape.

$$\mathrm{F}_{\sigma} = \sigma L \tag{1.3}$$

1.2.4 Interface

When a bubble approaches the interface, there is a film of heavy liquid between the bubble and the interface. This film is effectively stopping the bubble from passing the interface. The surface tension force produced by the interface and the buoyancy force produced by the bubble will cause the heavy liquid film in between to be drained. How fast the drainage mechanism is and thus how long the retention time will be depends on rheological properties of the used liquids and the size of the forces that are responsible for squeezing the heavy liquid. The approach speed of the bubble will also play a role since the impact will help the drainage of the heavy liquid film, again depending on driving force of the bubble and rheological properties of the liquid. System parameters that influence the passing of the bubble are the density of the phases, viscosity of the phases and the surface tensions between the phases. In Figure 1.4 a bubble at the interface and acting forces and system parameters can be seen.

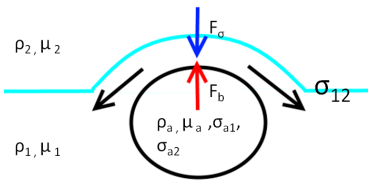

Figure 1.4: Bubble at the interface and the involved parameters and forces.

1.2.5 Dimensionless analysis

The system that is used in the experiments consists of a number of parameters. Describing these properties in dimensionless parameters is convenient when comparing certain conditions that are dependent on many parameters themselves. Expressing systems with dimensionless parameters is useful for analyzing and comparing since the result is a single dimensionless number depending on system parameters. First the systems parameters must be known in order to complete the dimensionless analysis. As was already introduced in section 1.2.4 the following system parameters are recognised:

$\rho_a, \rho_1, \rho_2, \sigma_{at}, \sigma_{ab}, \sigma_{tb}, \mu_t, \mu_b, \mu_a$. In this study the μ_a and ρ_a are neglected since there values are insignificant compared to the viscosity and density of the liquids. Since the experiments are conducted in a narrow column which influences drag forces, the column width W_c is also a parameter. Furthermore we study a bubble that is driven by density difference and gravitational force g, and the driving force depends on the bubble's diameter D_b. During the rise of the bubble, there is a speed in the bottom liquid u_b, in the top liquid u_t and a retention at the interface τ. Combining all parameters results in the following 13 parameters as can be seen in equation 1.4.

$$\text{system} = f(\rho_t, \rho_b, \sigma_{ab}, \sigma_{at}, \sigma_{tb}, \mu_t, \mu_b, W_c, D_b, g, u_b, u_t, \tau) \tag{1.4}$$

Non dimensionalizing (Hauke (2008)) can be done by determining the number of parameters (N) that a system depends on and by determining the SI units that make up these parameters (M). The parameters in this system depend on time, mass and length thus M is equal to 3. Any equation that links N dimensional parameters is equal to an equation that consists of N-M non dimensional parameters. Thus we can describe the system in 10 non dimensional parameters. Beginning with dimensionless numbers that describe inertial forces over viscous forces we have Re_{bottom} and Re_{top}, Reynolds can be seen in equation 1.5. The retention time is made non dimensional by substituting $\frac{D_b}{\tau}$ for the speed in the Reynolds number. Taking the inverse results in equation 1.6. Linking the two different viscosity's result in equation 1.7.

$$\text{Re} = \frac{F_I}{F_\mu} = \frac{\rho_l u D_b}{\mu} \tag{1.5}$$

$$\tau^* = \frac{\mu \tau}{\rho_l D_b^2} \tag{1.6}$$

$$\mu_{ratio} = \frac{\mu_t}{\mu_b} \tag{1.7}$$

The same is done for linking the different densities in a density ratio (1.8). Although this ratio describes the system, in this specific study it will be neglected. The ratio in the used multiphase systems varies between 1.07 and 1.31 which is compared to other dimensionless numbers a small difference and thus not used in this study.

$$\rho_{ratio} = \frac{\rho_t}{\rho_b} \tag{1.8}$$

Weber is useful in describing bubble shape since it relates to inertial forces over surface tension forces. The system has a bottom Weber We_b and a top Weber We_t, the Weber number can be seen in equation 1.9. At the interface body forces can be related to the surface tension force of the interface $\frac{F_b}{F_\sigma}$ resulting in the Eö number as can be seen in equation1.10. The surface tensions between liquid and air can be linked through a surface tension ratio (1.11).

$$\text{We} = \frac{F_I}{F_\sigma} = \frac{\rho u^2 D_b}{\sigma} \tag{1.9}$$

$$\text{Eö} = \frac{\delta \rho g D_b^2}{\sigma_{interface}} \tag{1.10}$$

$$\sigma_{ratio} = \frac{\sigma_1}{\sigma_2} \tag{1.11}$$

Finally the column width W_c and bubble diameter D_b can be related through a ratio as well (1.12). The system is now described with 10 dimensionless numbers as can be seen in equation 1.13. These dimensionless parameters will help during this study to describe the system.

$$wall_{ratio} = \frac{D_b}{W_c} \tag{1.12}$$

$$\text{system dimensionless} = f(Re_b, Re_t, \tau^*, We_b, We_t, Eö, \sigma_{ratio}, \rho_{ratio}, \mu_{ratio}, wall_{ratio}) \tag{1.13}$$

Chapter 2

Materials and Methods

2.1 Experimental setup

The experimental setup can be seen in Figure 2.1 and 2.2, a narrow column with D x W x H of respectively 5 mm, 150 mm and 470 mm was used. The orifice was attached at the centre of the bottom of the column. A Bronkhorst mass flow pump (MVP) was used to precisely control the flow rate of nitrogen through the orifice and to eliminate pressure drops in the gas chamber. The used flow rate was between 1 to 8 ml/hour for one MVP and 0.5 to 8 ml/min for the other MVP. A led panel was used to lighten the column. The bubble was captured by high speed imaging, a frame rate up to 1000 frames per second was achieved. The maximum resolution was 1920x1200 pixels. The used camera was a Basler acA1920-150uc. Two Basler's with different lenses were used, one with a 50 mm lens and a 20 mm extension and the other with a 12 mm lens and no extensions. The 12 mm camera made images with 12.8 pixels per mm. The column was filled up to 350 mm with the heavy phase and 50 mm of the light phase. A bubble was formed at an orifice with inner diameter of 0.25 mm, 1.02 mm and 2.00 mm. These orifices produced bubbles with diameter between 2.19 mm and 4.45 mm. For the step by step experimental procedure see appendix A.3 and for the cleaning procedure see appendix A.4

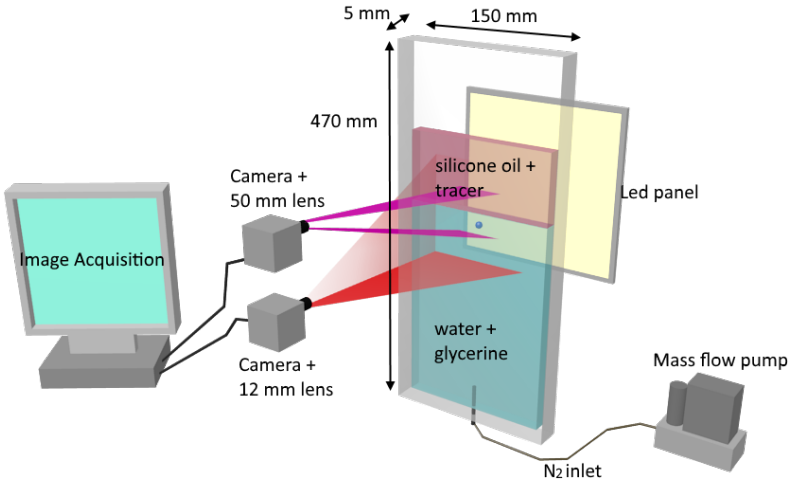

Figure 2.1: Schematic of the setup, this Figure is not to scale.

During the experiments two types of silicone oil were used as the light phase. For the heavy phase demi water and three different glycerine concentrations were used. The physical properties of the used Liquids are listed in Table 2.1. The surface tensions between the heavy phase and the light phase are listed in Table 2.2.

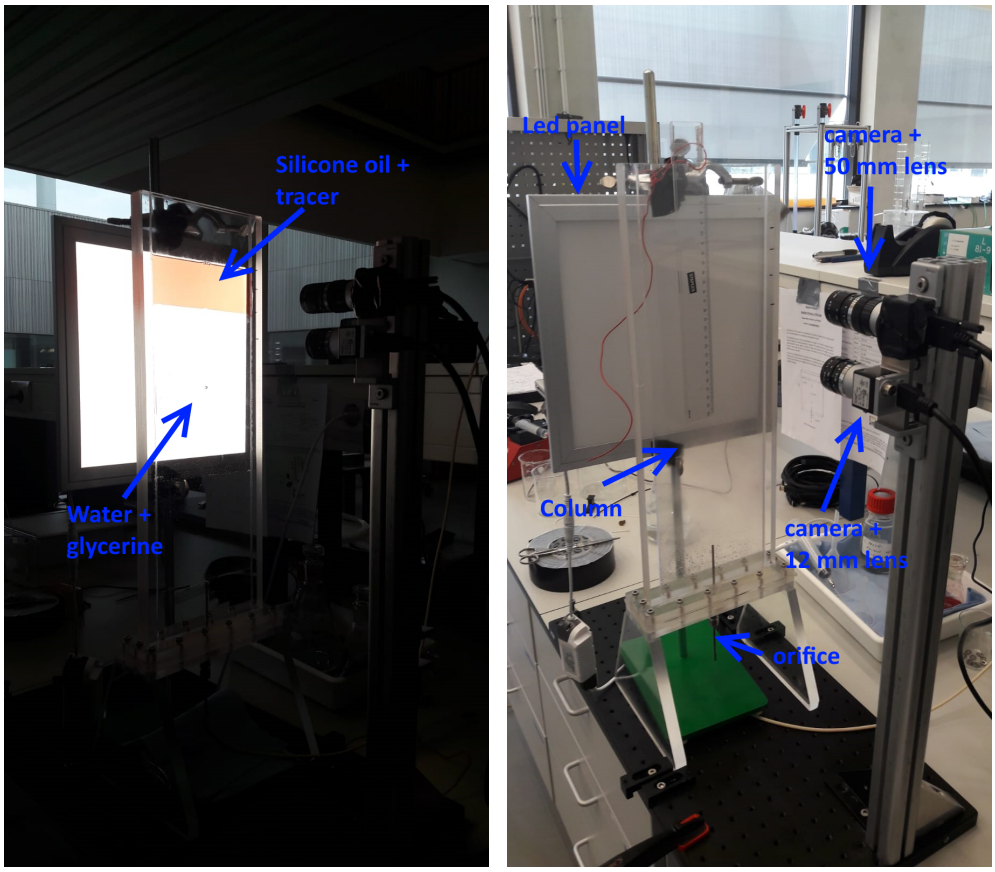

(a) (b)

Figure 2.2: The actual setup can be seen in this Figure.

Table 2.1: Used phases and their physical properties, the viscosities and surface tensions of the glycerine concentrations were determined with the Table Gly. The properties of the silicone oil were determined with Bonhomme et al. (2012).

Liquid	$\rho(kg/m^3)$	$\mu(mPa.s)$	$\sigma(mN/m^2)$
water	997	1.002	71.7
glycerine 53%	1139	7.4	68.3
glycerine 85%	1224	109	64.8
glycerine 92%	1245	310	63.6
silicone oil 10 cSt.	932	9.6	20.2
silicone oil 350 cSt.	968	375	20.9

Table 2.2: Used multi phase systems and their interfacial surface tensions, these were determined with Bonhomme et al. (2012).

multi phase system($\sigma_{tb}(mN/m^2)$)	silicone oil 10 cSt.	silicone oil 350 cSt.
water	19.7	13.9
glycerine 53%	25.4	23.9
glycerine 85%	28.8	29.9
glycerine 92%	28.1	28.3

2.2 Bubble volume

Bubbles have a shape ranging from spherical to ellipsoidal. To determine the volume and diameter of the bubble, one should take into account that the column width is 5 mm. This is the same order of magnitude as the bubbles and wall effects will cause that the diameter of the bubble in the length is not equal to that in the width, as is assumed when studying bubbles in infinite medium. Due to the fact that images are two dimensional, one can determine a bubbles horizontal diameter and vertical diameter. To calculate the diameter in the width there are two separate methods. The first method assumes that bubbles are spherical. This is the case for low Reynolds. To calculate the equivalent diameter, corresponding to that of a perfect sphere, we assume that the horizontal diameter is also the diameter of the bubble in the width and thus the formula for calculating bubble diameter (2.1) and bubble volume (2.2) becomes as follows:

$$D_{eq} = \sqrt[3]{d_v d_h^2} \tag{2.1}$$

$$\mathrm{V} = \frac{1}{6}\pi d_v d_h^2 \tag{2.2}$$

This approach works well only when bubbles are spherical, but when bubbles have strong oscillations and ellipsoidal shape this method becomes flawed. As mentioned earlier the column will have a certain effect on the unknown diameter as well. The second more accurate method to determine bubble volume is by using a constant flow rate when producing bubbles and by doing a frequency measurement of the bubbles with known flow rate. The volume can be calculated as can be seen in equation 2.3. And the equivalent diameter becomes as can be seen in equation 2.4.

$$\mathrm{V} = \frac{F_{gas}(ml/min)}{f_{frequency}} \tag{2.3}$$

$$D_{eq} = \sqrt[3]{\frac{6 * V}{\pi}} \tag{2.4}$$

However a constant flow rate is not always practical. After bubbles pass the interface, the interface gets disturbed and needs to be stirred in order to restore to its initial state. With a constant flow rate that is too high, there is not enough time to restore the interface and successive bubbles will not pass through a straight interface. The experiments conducted with a heavy phase of water, glycerine 53% and glycerine 85% with an orifice of inner diameter of 2 mm made use of a MVP with flow rates between 0.5-8 ml/min. Due to the high flow rate, constant flow was not possible and after each bubble the flow rate was stopped. It was observed that the first bubble produced when operating the MVP had a volume that was bigger than that of the successive bubbles and thus equation 2.3 did not apply for the first produced bubble. For these experimental sets diameter and volume were determined with equation 2.1 and equation 2.2. For all other systems a MVP was used with flow rate between 1-8 ml/hour, giving the possibility to set flow rate low enough to maintain constant flow and have enough time to restore the interface to its initial state. In those cases equation 2.3 and equation 2.4 were used to calculate volume and equivalent diameter.

2.3 Refractive index

When making a solution of technical glycerine with water, this is done by weighting the needed mass on a scale before mixing the two fluids. It is necessary to determine the refractive index of the solutions since the technical glycerol is not 100 percent pure and the scale has an error margin as well. Since the viscosity of glycerine concentrations increase on a logarithmic scale, a relatively small difference in concentration can cause significant difference in viscosity. The properties of the used heavy phases and the technical glycerol are listed in the Table 2.3.

Table 2.3: Refraction of used heavy phases determined with a Refractometer. The corresponding concentration was determined with the Table Ref. The corresponding viscosity was determined with the booklet Gly.

index	glycerine(%)	viscosity(mPa.s)
133.3	0	1
140.2	53	7.4
145.1	85	109
146.1	92	310
147.3	99	1150

2.4 Image processing

The images were processed in order to obtain data out of them. For this purpose FIJI (Schindelin et al., 2012) was used, which is an open source distributor of ImageJ. The processing steps that were taken are shown in Figure 2.3. The steps are as follows:

- An image stack is imported into FIJI (2.3a).
- The stack was converted into 32 bit since only contrast was needed and no colours (2.3b)
- The background of the 32 bit image stack was subtracted with a sliding paraboloid to remove noise (2.3c).
- Since the bubble had motion and the interface and reverence point are standing still, all pixels that are not changing intensity were removed by making a maximum intensity z projection of the stack and subtracting that from the original stack (2.3d).
- The object (bubble) was isolated and the boundary was enhanced by converting the stack into 8 bit and adjusting the threshold, resulting into a binary image stack (2.3e).
- The object was filled with the binary operation fill holes (2.3f).
- An ellipse was fitted around the object (2.3g).
- The stack was processed and the ellipsoids can be seen over time (2.3h).

From this final image stack the following data was extracted: the area, the x and y position of the centre of the fitted ellipse, the major and minor diameter of the fitted ellipse and the angle of the fitted ellipse. The positions were used to calculate speeds and obtain position plots. The diameters were used to calculate the volume and shape factor. This data was processed with Python® as can be seen in section 2.5.

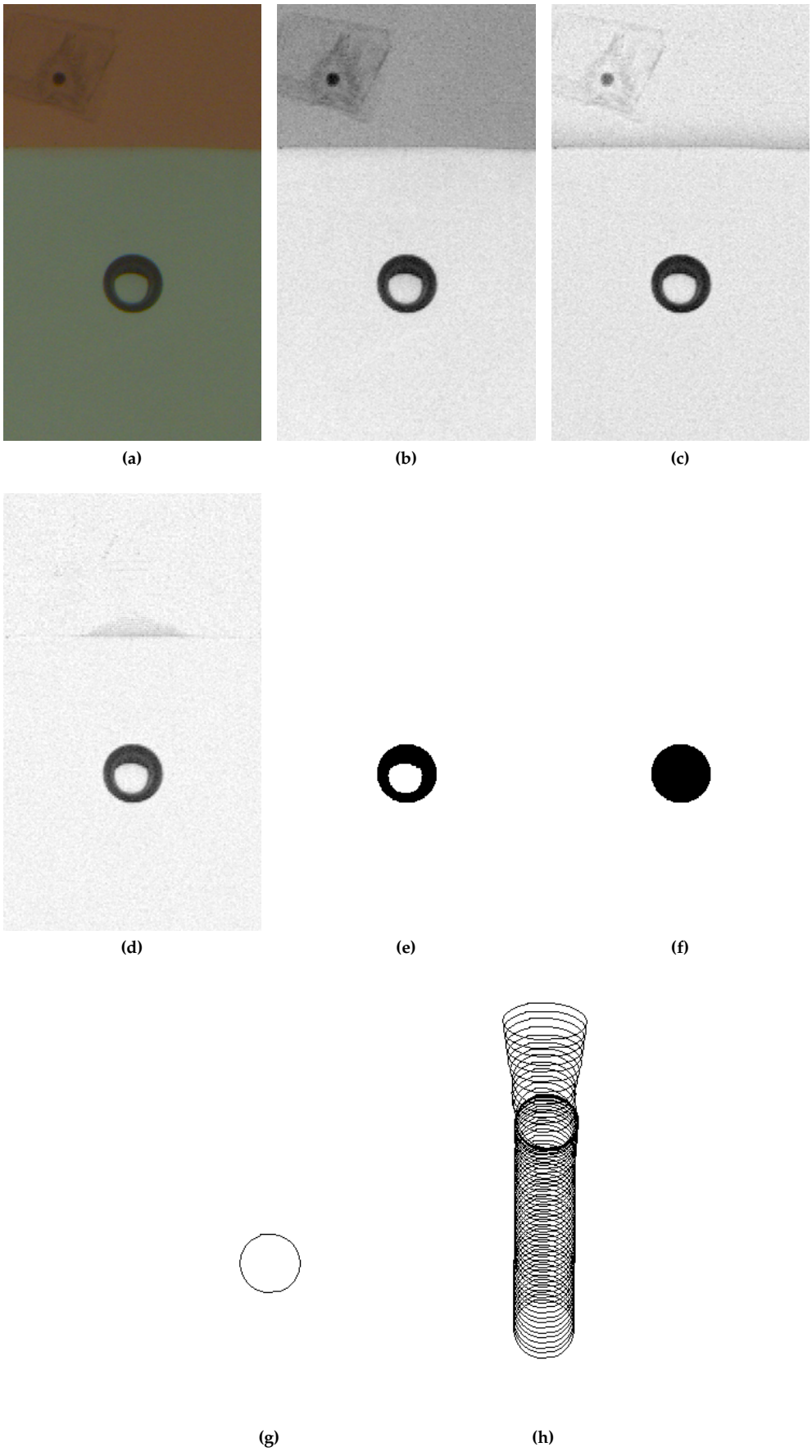

Figure 2.3: Processing steps of an image stack: 2.3a) original image, 2.3b) converted to 32 bit, 2.3c) background subtracted, 2.3d) max intensity z projection subtracted, 2.3e) image binarized with thresholding, 2.3f) filled holes with binary operation,2.3g) fitted an elipse, 2.3h) processed stack over time to obtain data.

2.5 Data processing

From FIJI data of the rising bubbles are obtained. The data files contain 7 columns consisting of: sequence, area, x-position, y-position, major diameter, minor diameter and the angle of a fitted ellipse. These data files are processed with a Python® script. The script makes Plots to analyse the data including height, speed, shape factor and position of each individual bubble over time as can be seen in Figure 2.4.

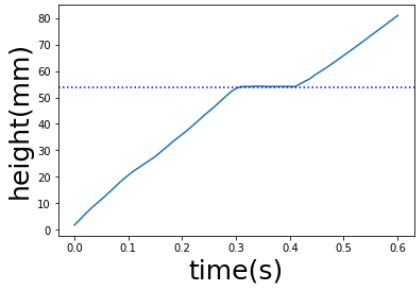

(a) height of the centre of a fitted ellipse over time

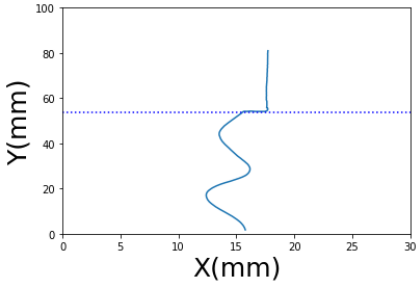

(b) position of the centre of a fitted ellipse over time

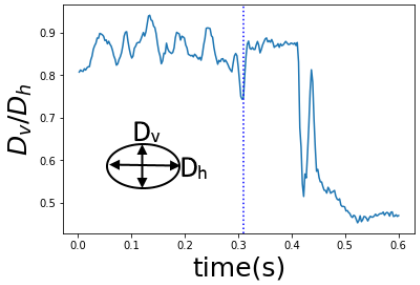

(c) shapefactor over time

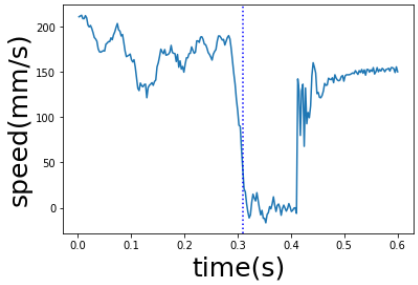

(d) speed over time

Figure 2.4: Plots of data files for analysis purposes. The interrupted line represents the interface.

To calculate the interface height, a matrix of intensity values of an 8 bit image is loaded in Python. The reason for not calculating the height with for example Figure 2.4b is that the interface will be elevated once a bubble is present. The amount of elevation varies across the different conditions and to make sure to capture the original interface height, an intensity matrix is used. A list is obtained that contains all intensity values of the middle pixels from top to bottom. In Figure 2.5 the intensity of the pixels can be seen. At a certain point there is an intensity increase that represents the transition from top to bottom phase. A threshold value is given. The threshold is met when intensity increases and the particular pixels at which the threshold intersects is recognized as the height of the interface. The interface height can thus be plotted together with other data as can be seen in Figure 2.4a and 2.4b.

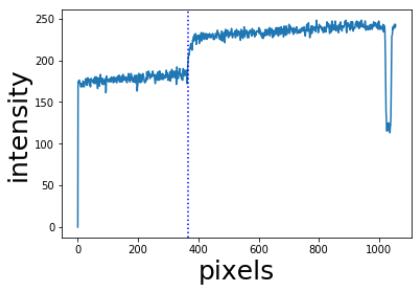

Figure 2.5: The intensity of all pixels in the middle of a picture from top to bottom

To obtain the average shape factor, average speed and average retention time, the rising of the bubble is

divided into three zones: before interface, at interface and past interface. The speed drops significantly when the interface is reached and increases after passing the interface as can be seen in Figure 2.4d. Two threshold speeds are set to recognize when the bubble decelerates and accelerates and thus enables to divide the rising bubble into the three zones. In each zone the average is calculated by enumerating the data and dividing over the number of data points. The frequency at which the high speed imaging is taken is known and thus it is possible to calculate time by multiplying the number of data points by the camera frequency. The experiments were conducted in sets of 5 and thus the standard deviation was calculated as can be seen in equation 2.5.

$$\mathrm{SD} = \sqrt{\frac{\sum(x-\mu)^2}{n-1}} \tag{2.5}$$

When plotting datasets together they must be normalized. The pictures of the different bubbles in each set were taken without changing the camera position. In order to normalize the graphs and set the starting point, the python script plots data starting from an initial height. Since the experiments were conducted in sets, each dataset was plot together to obtain the normalized plots as can be seen in Figure 2.6. All normalized plots are available in appendix A.

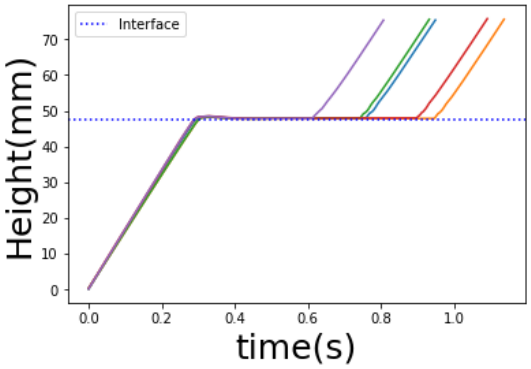

Figure 2.6: Height over time for a dataset of five.

Chapter 3

Results and Discussion

3.1 Retention time at the interface

Before a bubble passes the interface, it is retained due to the heavy liquid film effectively stopping the bubble from rising. Retention time changes in different viscous bottom liquids as can be seen in Figure 3.1. The top liquid is in both cases silicone oil 350cSt. and the bottom liquid consists in one case of pure demi-water and in the other case of glycerine 92%. The bubbles have equivalent diameter of 4.01 and 3.46 mm. Viscosity is 1 and 109 cSt. respectively. The measured retention times are 0.10 s and 8.2 s respectively. It can thus be stated that the viscosity of the bottom liquid has a significant influence on the bubble's retention time. In more viscous liquid, bubbles have lower velocity and thus there is less drainage at impact with the heavy liquid film. Also when the heavy liquid film is squeezed between the bubble and the interface, the rate at which this drainage occurs is dependent on the liquids rheological properties since a more viscous liquid film has more difficulty to flow and thus the drainage time at the interface is therefore increased.

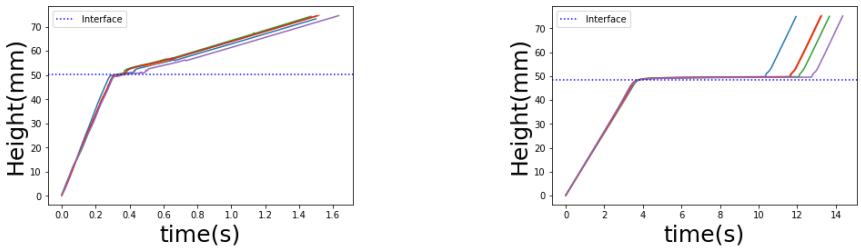

(a) water-sil 350cSt,$D_b = 4.01mm$ **(b)** gly 92%-sil 350cSt,$D_b = 3.46mm$

Figure 3.1

When the bottom and top liquid are left unchanged and the bubble size is decreased, in most cases an increase in retention time is observed. In Figure 3.2 two cases with the same liquids and different bubble sizes can be seen. The equivalent bubble diameter is 3.46 mm and 2.75 mm and the retention time is 8.2 and 10.7 s respectively. Bubbles with less buoyancy force are slower due to having a bigger surface area in relation to their volume and thus drag forces become more dominant. Thus the impact of a smaller bubble with the heavy liquid film causes less drainage and since the forces involved in squeezing the interface are smaller, drainage at the interface will take more time. Thus retention time increases with decreased bubble size as was also concluded by Kemiha et al. (2007). There where however cases were smaller bubbles in the same conditions did not have higher retention time and sometimes even lower retention time. It should be considered that the thickness of the column is 5 mm and bubbles with diameters of more than 4 mm were produced. These bubbles will be more influenced by wall effects than smaller bubbles and their drag force is higher than would be in infinite medium. Smaller bubbles are expected to have lower speed whereas this is not always the case in this study. For example in water-silicone oil 10 cSt. the speed of the 4.11 mm, 3.08 mm and 2.26 mm bubbles are respectively 0.174 m/s,

0.178 m/s and 0.180 m/s as can be seen in Table A.1. The 2.26 mm bubble actually has the highest speed which helps drain the heavy liquid film at impact.

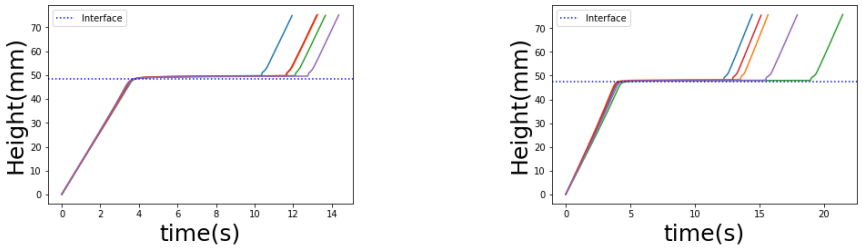

(a) gly 92%-sil 350cSt,$D_b = 3.46mm$ **(b)** gly 92%-sil 350cSt,$D_b = 2.75mm$

Figure 3.2

Retention time is influenced by viscosity of the bottom liquid, the approach speed of the bubble and the equivalent diameter of the bubble. The Reynolds number of the bottom liquid Re_b (equation 1.5) is used as the main parameter of the system to describe retention time, since the most important parameters that influence retention time are present in the Reynolds number. For each of the twenty datasets the Re_b is calculated and plotted against the retention time as can be seen in Figure 3.3. The Figure shows that a higher Reynolds number results in lower retention time. This trend describes the entire system and is in agreement with the previous observations: smaller bubbles cause lower Reynolds resulting in higher retention time, faster bubbles causes higher Reynolds and lower retention time and more viscous liquid will result in lower Reynolds and higher retention time.

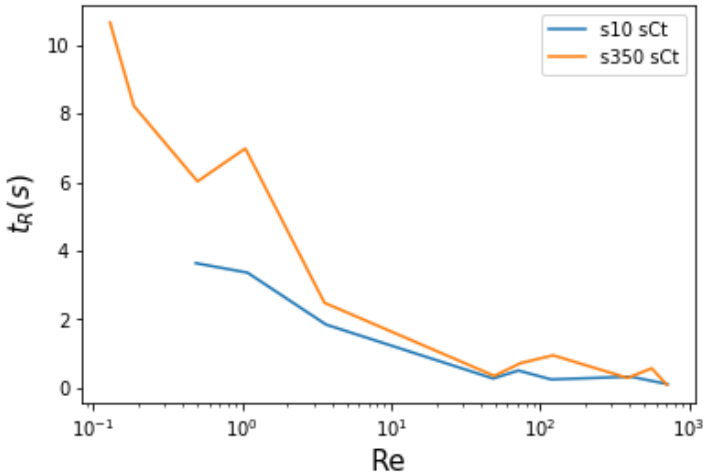

Figure 3.3: The Retention time vs Reynolds number can be seen in this figure. The blue line represents Re_b with a 10 cSt. top liquid and the orange line represents Re_b with a 350 cSt. top liquid.

In Figure 3.4 Reynolds against retention time can be seen including the deviation. It is observed that a more viscous top layer at equal bottom Reynolds causes a slight increase in retention time. In theory when the top liquid is less viscous, this allows for more room of the bottom liquid to push away top liquid and thus drainage can be increased. At low bottom Reynolds, a more viscous top liquid indeed seems to significantly increase retention time. However at high Reynolds numbers, deviation shows overlap and the influence of the top liquid is not significant.

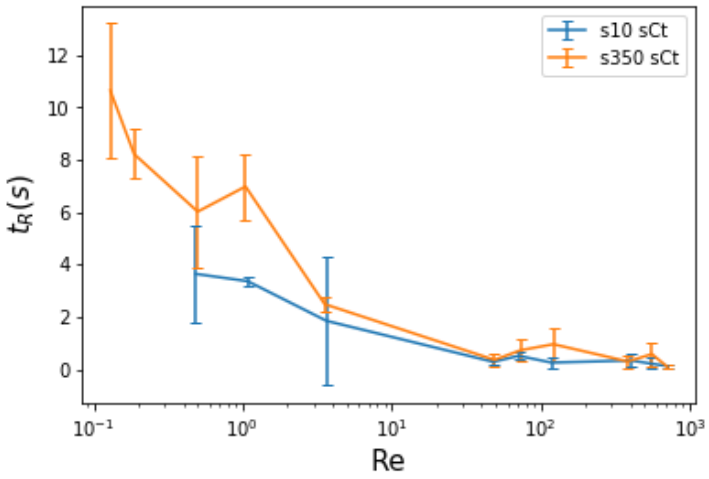

Figure 3.4: Retention time vs Reynolds and the corresponding deviation can be seen in this figure.

3.1.1 Deviation retention time

In Figure 3.4 it can be seen that certain experiments had more deviation than others. In Figure 3.5 the height over the time of two sets can be seen. The bubbles have diameters of 2.26 mm and 2.20 mm, which is relatively small. Figure 3.5a shows a wide range of retention times, whereas Figure 3.5b shows that the range of retention times is narrow, except for one deviant bubble. The deviation divided by the mean of these two figures are 0.72 and 0.35 respectively. Factors that account for deviation are that bubble size has a slight variation, speed of each bubble has a slight variation as well and in less viscous liquids bubbles have relatively large oscillations that are uncontrollable. The interface between the two liquids is not entirely straight but has small variations as well, which influences retention time. Smaller bubbles were more sensitive to small changes causing more deviation than larger bubbles. A more viscous bottom liquid causes relative deviation to be smaller as can be seen in Figure 3.5.

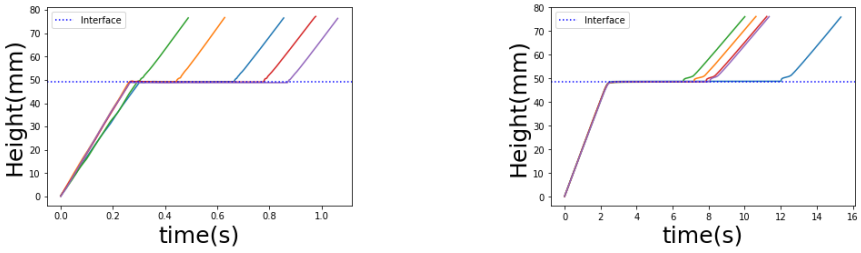

(a) water-sil 10cSt,$D_b = 2.26mm$ **(b)** gly 53%-sil 10cSt, $D_b = 2.20mm$

Figure 3.5: In this Figure the bubble size between both plots is kept constant and the bottom liquid viscosity is varied, causing very different deviations.

3.2 Entrainment of heavy liquid

Most of the bubbles passing the interface did not cause entrainment of heavy liquid into the light phase except for two condition. The 4.45 mm bubbles in glycerine 85% with silicone oil 350 cSt. and the 4.27 mm bubbles in glycerine 53% with silicone oil 10 cSt. encapsulated the heavy liquid after the bubbles passed the interface. Figure 3.6 displays a rising bubble that did not cause encapsulation, the observation is that the bubble reaches the interface and comes to an abrupt stop. Then the bubble completely drains the heavy liquid film before penetrating the interface and rising through the top liquid. In Figure 3.7 encapsulation of the bubble can be seen, it is observed that the bubble does not penetrate the interface

but deforms it significantly and eventually remains encapsulated by the heavy liquid. The bubble did not come to a complete halt but kept rising at a certain speed when at the interface.

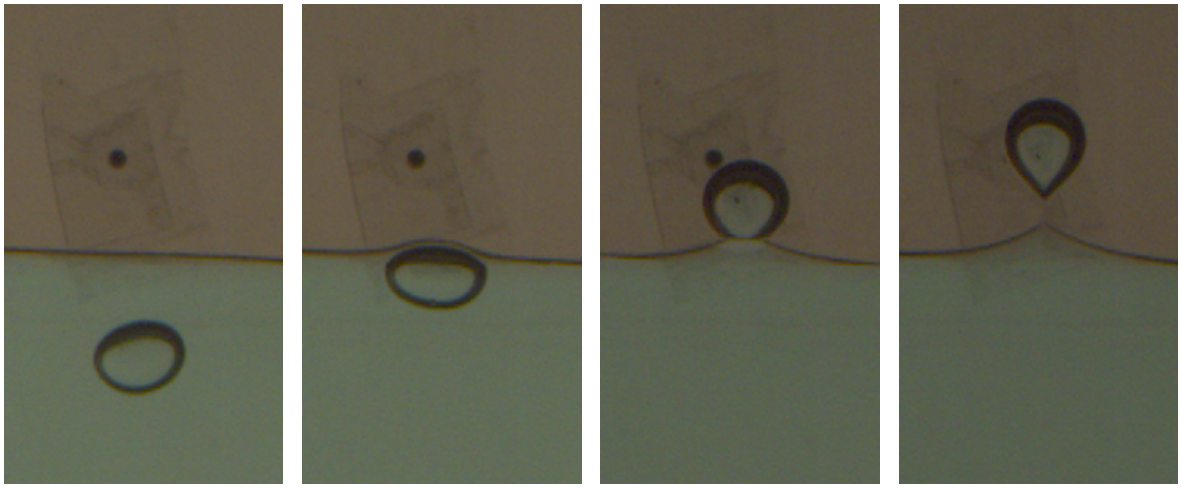

(a) (b) (c) (d)

Figure 3.6: A bubble passing through the interface. The heavy phase consists of water and the light phase consists of silicone oil 350 cSt.

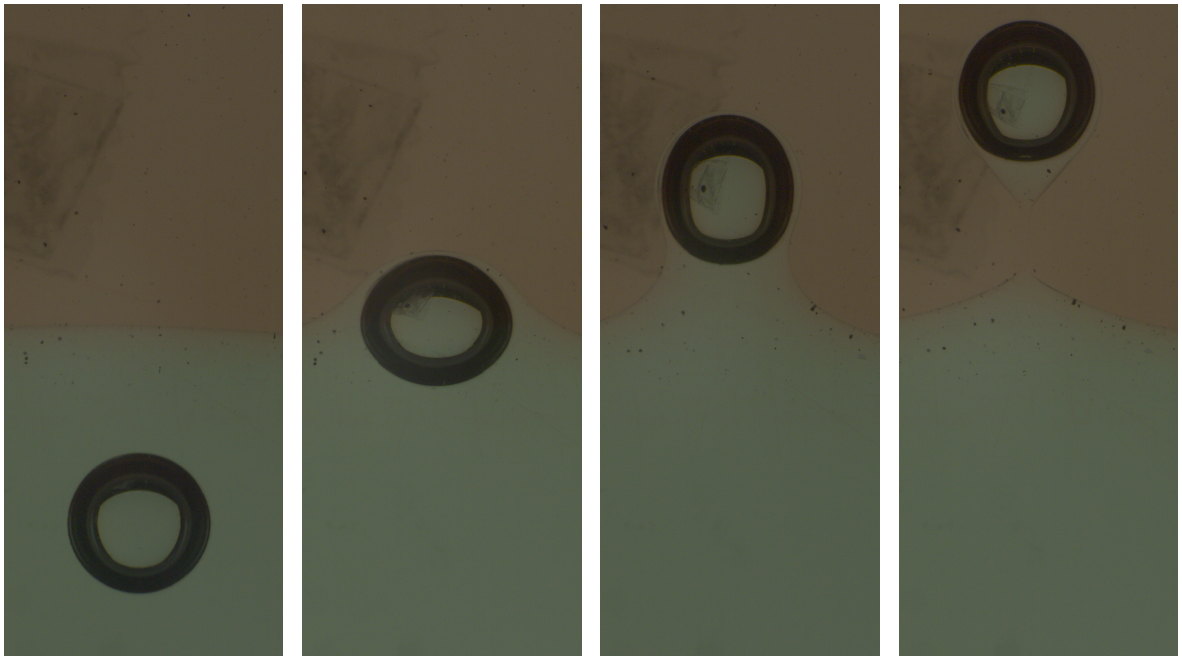

(a) (b) (c) (d)

Figure 3.7: A bubble passing through the interface being encapsulated by heavy liquid. The heavy phase consists of glycerine 85% and the light phase consists of silicone oil 350 cSt.

Encapsulation was only observed with bubbles above 4 mm and it can thus be concluded that buoyancy force plays a role in this phenomena. Since the bubble deforms and passes an interface, the surface tension force is an important parameter as well. To study the effect of buoyancy force relative to surface tension force the Eötvos number as described in equation 1.10 is used. As can be seen in Table A.1 the bubbles that have observed encapsulation have Eö numbers of 0.796 and 0.803 respectively. There are still other

experimental conditions in which the Eö number is above 0.8 but no encapsulation is observed and thus this phenomena cannot solely be explained with Eö numbers. An interesting observation about the two encapsulation cases is that they both happen in different viscosity regimes. glycerine 53% being 15 times less viscous than glycerine 85% and silicone oil 10 cSt. being 39 times less viscous than silicone oil 350 cSt. Encapsulation happens at different bottom and top viscosities and thus an interesting number to look at is the ratio between the viscosity of the top liquid and bottom liquid (1.7). In A.1 the viscosity ratios are listed between the top and bottom liquid. The two cases were encapsulation happened have viscosity ratio 3.44 and 1.30 respectively. How the viscosity ratio should be interpreted is as a similarity between flow properties between the two liquids and for encapsulation to happen there should be reasonable similarity between the two liquids. In case of glycerine 92%-silicone oil 350cSt and 3.46 mm bubbles the viscosity ratio was 1.21 and the Eö number was 0.516 but no encapsulation was observed. meaning that Eö was not large enough and despite the viscosity ratio being near unity there was thus no encapsulation. To clarify the role of Eötvos and viscosity ratio, Figure 3.8 can be seen. From this Figure it is clear that Eö needs to be at least 8 and the viscosity ratio must be near unity for encapsulation to take place.

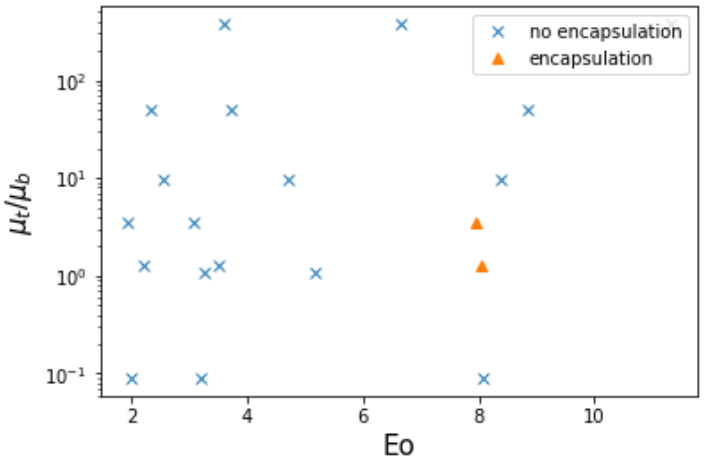

Figure 3.8: Viscosity ratio vs Eötvos number, displaying whether there is encapsulation or no encapsulation.

This study tried to combine the most important dimensionless parameters in order to describe the passing phenomena of a bubble. The retention time is one of the passing phenomena and the dimensionless retention time is used to describe the system. Furthermore body forces play a role when the bubble elevates and encapsulates the interface. To describe the body forces, the Eötvos number was used. In Figure 3.9 and 3.10 dimensionless retention time is plotted against Eötvos. The lines are viscosity ratios, which describe the liquid properties. The figure empirically displays the passing of the bubble at the interface. At low Eötvos the interface remains flat. Increasing the Eötvos number also increases elevation of the interface. In certain conditions at viscosity ratios near unity and Eö above 8, encapsulation takes place. In Figure 3.9 the top liquid has a viscosity of 375 cSt. and the bottom viscosity is changed in order to obtain the different ratios. In Figure 3.10 the viscosity of the top liquid is 9.6 cSt.

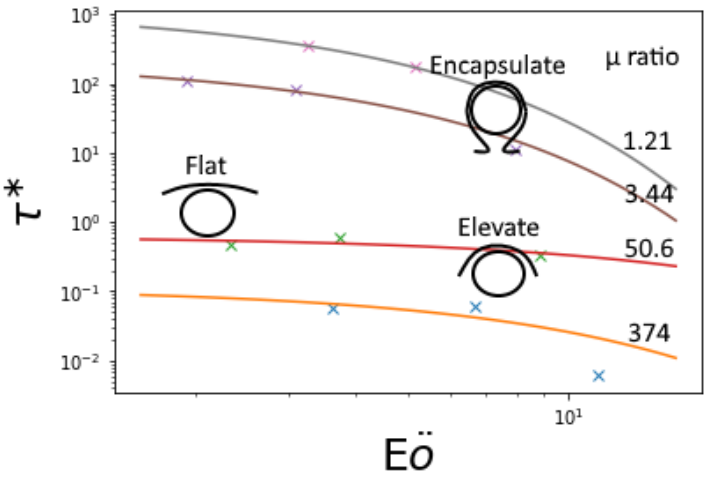

Figure 3.9: Eötvos number vs. dimensionless retention time (equation 1.6). An empirical map can be seen where the shape of the interface and the passing phenomena is visually displayed. The used top liquid is silicone oil 350 cSt. The ratios were obtained by varying the bottom liquid viscosity.

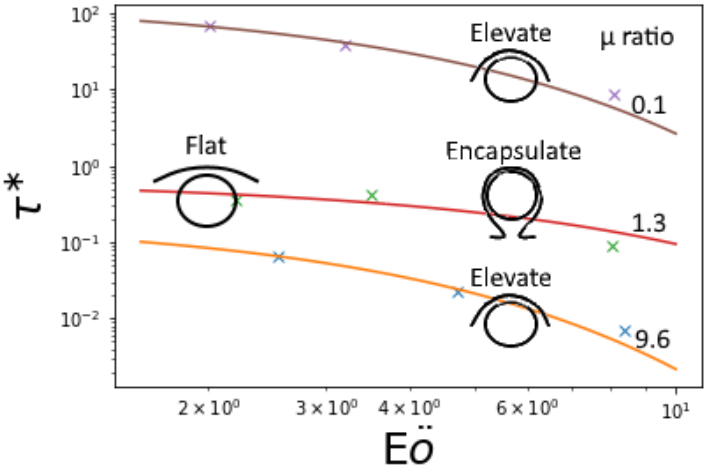

Figure 3.10: Eötvos number vs. dimensionless retention time (equation 1.6). An empirical map can be seen where the shape of the interface and the passing phenomena is visually displayed. The used top liquid is silicone oil 10 cSt.The ratios were obtained by varying the bottom liquid viscosity.

3.3 Shape of the bubble

Bubbles can take many shapes depending on the liquid there surrounded with. In Figure 3.11 you can see the various bubble shapes in different conditions where viscosity is 109, 1 and 9.6 mPa/m respectively. The speed for each of the three cases is 0.174 , 0.074 and 0.132 m/s respectively. Whereas the shape factor is 0.81, 0.98 and 0.38 respectively. Besides the speed, surface tension should be considered as well since the shape depends on balance between the inertial forces that deform the bubble and surface tension forces that try to minimize the surface area between the bubble and the liquid. Smaller bubbles were observed to have more spherical shape since there surface area to body ratio is larger relative to that of larger bubbles.

(a) g85, $D_b = 4.40mm$ **(b)** water, $D_b = 4.11mm$ **(c)** s10 cSt, $D_b = 4.11mm$

Figure 3.11: Shape of bubbles in different conditions.

The shape of a bubble is dependent on the surface tension forces relative to the inertial forces. The Weber number is therefore used to describe the shape factor of the bubbles. In Figure 3.12 the shape factor vs. the Weber number can be seen for all the conducted experiments. It can be seen that higher Weber numbers result in a lower shape factor.

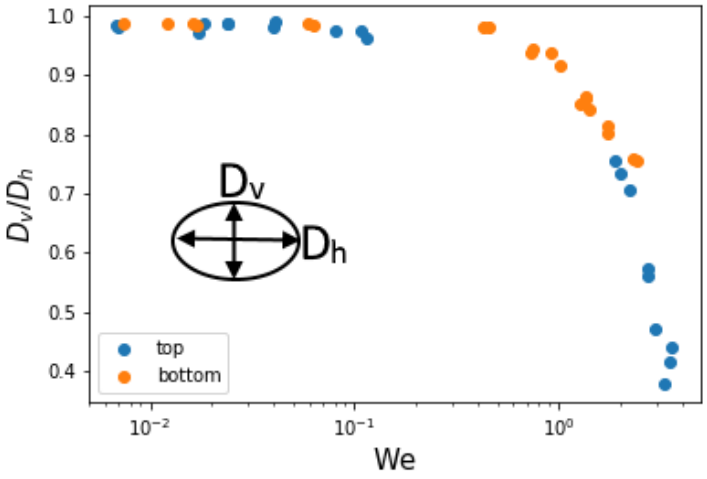

Figure 3.12: Shape factor vs weber number can be seen in this figure.

Moore (1965) has found a simple correlation between shape factor and Weber number at low deformations in infinite medium. Moore's correlation as used in this study can be seen in equation 3.1. In Figure 3.13 the experimental results are plotted together with Moore's correlation. Indeed at lower Weber numbers with smaller deformations the equation fits well.

$$\chi = \frac{1}{1 + \frac{9}{64}We} \tag{3.1}$$

Legendre et al. (2012) tried to describe the shape factor with the Morton and Weber number. For the studied conditions, the theoretical shape factor was calculated with Legendre's equation 3.2 and where plotted against the experimental data in the same Figure as Moore. As can be seen the fit is not significantly different than from Moore's fit in Figure 3.13.

$$\chi = 1 - \frac{9}{64}We(1 + K(Mo)We)^{-1} \tag{3.2}$$

$$K(Mo) = 0.2Mo^{1/10} \tag{3.3}$$

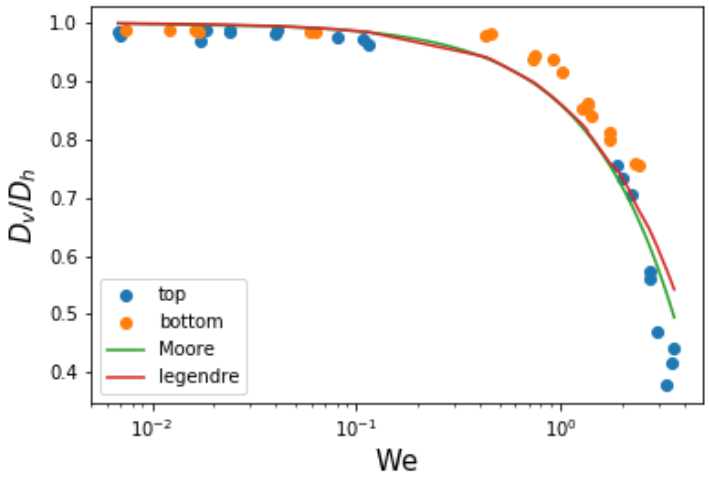

Figure 3.13: Shape factor vs weber number can be seen in this figure, Moore's and Legendre's equations are included.

The correlations of Moore and Legendre were both for infinite medium and from the plot it can be concluded that also in a narrow column, there correlations describes the bubble shape well.

Chapter 4

Conclusion and recommendation

4.1 Conclusion

The passing phenomena of a rising gas bubble through a liquid-liquid interface was studied in a narrow column with high speed imaging. The viscosity ratio and size of the bubbles were varied and the effect on retention time, heavy liquid entrainment and bubble shape were studied. The following conclusions resulted from this study:

- When the bubble has a higher approach speed or if viscosity of the bottom liquid is decreased, the retention time will decrease. Increased equivalent diameter results in lower retention time. The retention time can be described with the Reynolds number of the bottom liquid. Higher Reynolds number result in lower retention time.
- Encapsulation of heavy liquid happens when viscosity ratio nears unity and when Eötvos number is higher than 8. Encapsulation is dependent on the rheological properties of both the bottom and top liquid and body forces need to be sufficient for encapsulation to take place. A higher Eötvos number results in a more elevated interface.
- The shape factor decreases when inertial forces become more dominant over the surface tension force. The shape factor can be described with the Weber number whereby a higher Weber number results in lower shape factor.
- The equations of Moore and Legendre represent well the relation between the Weber number and shape factor at low Weber numbers and becomes slightly less representable at higher Weber numbers. The correlations prooved usefull in a narrow column.

4.2 Recommendation

Encapsulation was observed at Eötvos numbers of 8 and it is assumed that higher Eö at viscosity ratio's near unity would show encapsulation. This needs further research by setting up experiments in higher Eötvos regimes in order to validate this assumption. Another interesting study would be the effect of viscosity of the top liquid on retention time at Reynolds numbers of the bottom liquid above 10. Are the effects of more viscous top liquid still insignificant at these high Reynolds numbers even if experiments are conducted at extreme top liquid viscosity? At last the setup made use of a narrow column and the bubbles speed and retention time were to a certain extent subject to wall effects. The influence of wall effects on bubble speed and retention time are not jet exactly known and research that focuses directly on wall to bubble ratios could give more clarity of the wall effects on retention time.

Acknowledgements

This project has been very interesting and educational. During my bachelor the main focus has been chemistry and at the department of Transport Phenomena I learned new insights about physics and gained more knowledge about transport phenomena. I would first like to thank Dr. Luis Portela for his insights and discussions and of course for enabling this project in the first place. I would also like to thank my daily supervisor Manas Mandalahalli for his assistance and supervision during my bachelor thesis.

Bibliography

Physical properties of glycerine and its solutions. URL https://www.aciscience.org/docs/Physical_properties_of_glycerine_and_its_solutions.pdf.

refractive index of glycerin-water solutions at 20 °c. URL http://edge.rit.edu/edge/P13051/public/Research%20Notes/refractive%20index%20glycerin%20water.pdf.

R. Bonhomme, J. Magnaudet, F. Duval, and B. Piar. Inertial dynamics of air bubbles crossing a horizontal fluid-fluid interface. *Journal of Fluid Mechanics, Cambridge University Press (CUP), vol. 707*, pages 405–443, 2012.

R. Clift, J.R. Grace, and M.E. Weber. *Bubbles, drops, and particles*. ACADEMIC PRESS, INC, 1978.

G. Hauke. *An Introduction to Fluid Mechanics and Transport Phenomena*. Springer, 2008.

M. Kemiha, E. Olmos, F. Fei, S. Poncin, and H.Z. Li. Passage of a gas bubble through a liquid-liquid interface. *Ind. Eng. Chem. Res. 46*, pages 6099–6104, 2007.

D. Legendre et al. On the deformation of gas bubbles in liquids. *Phys. Fluids 24, 043304*, 2012.

D. W. Moore. The velocity of rise of distorted gas bubbles in a liquid of small viscosity. *J. Fluid Mech. 23, 749*, 1965.

C.P. Ribeiro Jr. Gas-liquid direct-contact evaporation. *Chem. Eng. technol. 28*, pages 1081–1107, 2005.

J. Schindelin, I. Arganda-Carreras, E. Fride, et al. Fiji: an open-source platform for biological-image analysis. *Nature methods 9(7)*, pages 676–682, 2012.

K. Shimizu, S. Takada, K. Minekawa, and Y. Kawase. Phenomenological model for bubble column reactors: prediction of gas hold-ups and volumetric mass transfer coefficients. *Chem. Eng. J. 78*, pages 21–28, 2000.

K.K. Sing and Hans-Jörg Bart. Passage of a single bubble through a liquid-liquid interface. *Ind. Eng. Chem. Res.*, 2015.

P. Snabre and F. Magnifotcham. Formation and rise of a bubble stream in a viscous liquid. *Eur. Phys. J. B 4*, pages 369–377, 1998.

D. Y. Song, N. Maruoka, H. Shibata, S. Kitamura, and N. Sasaki. Influence of bottom bubbling rate on formation of metal emulsion in sn-sb-cu alloy and molten salt system. *ISIJ International, Vol. 57 , No. 2*, pages 236–244, 2017.

H.E.A. van den Akker and R.F. Mudde. *Transport verschijnselen*. Delft university press, 1996.

Appendix A

Appendix

A.1 Height plots

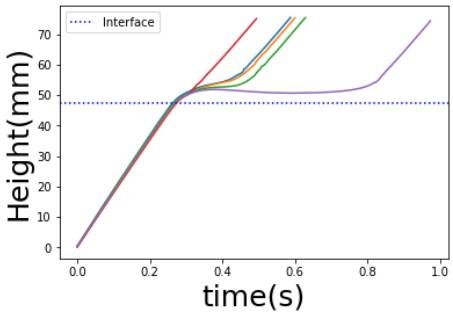

Figure A.1: g53-s10, $D = 4.27mm, \sigma = 0.75$

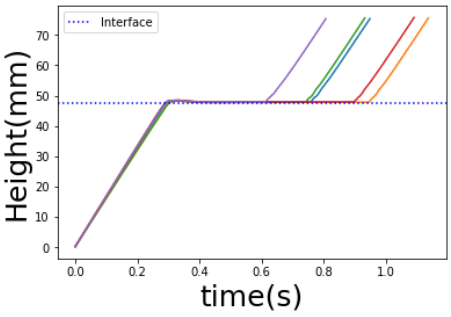

Figure A.2: g53-s10, $D = 2.82mm, \sigma = 0.26$

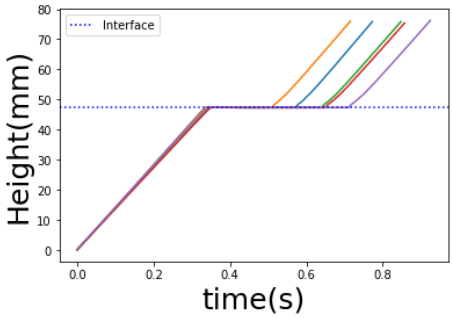

Figure A.3: g53-s10, $D = 2.23mm, \sigma = 0.27$

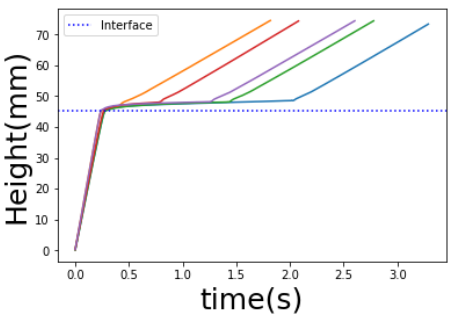

Figure A.4: g53-s350, $D = 4.35mm, \sigma = 0.65$

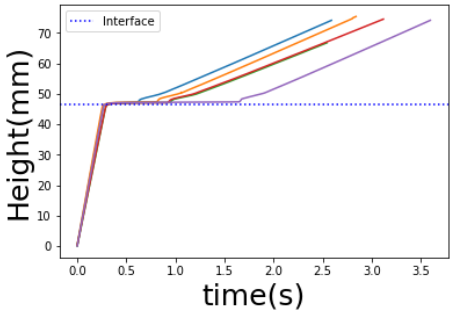

Figure A.5: g53-s350, $D = 2.82mm, \sigma = 0.54$

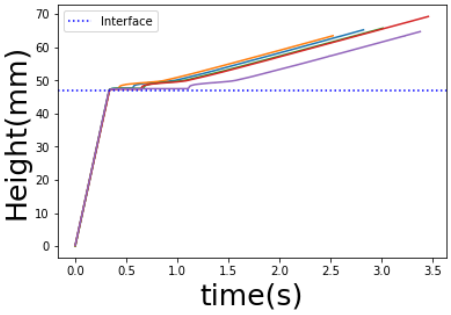

Figure A.6: g53-s350, $D = 2.23mm, \sigma = 0.72$

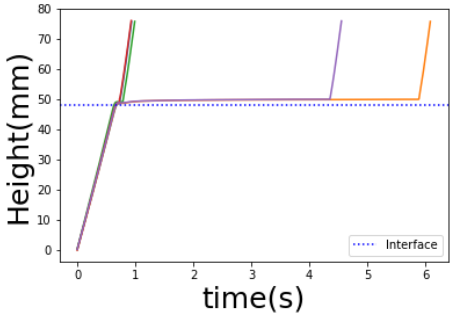

Figure A.7: g85-s10, $D = 4.40mm, \sigma = 1.32$

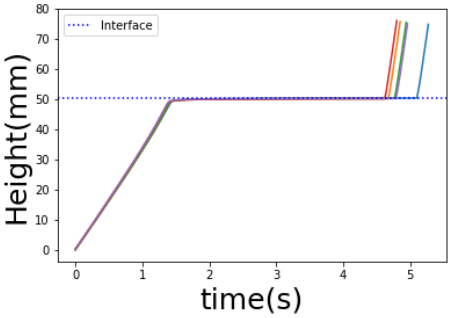

Figure A.8: g85-s10, $D = 2.77mm, \sigma = 0.05$

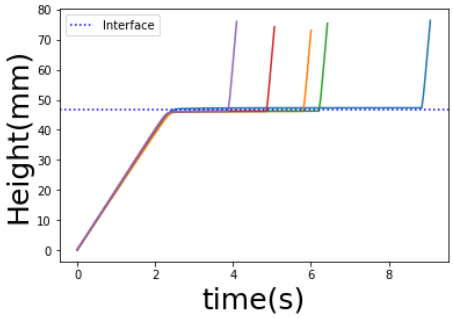

Figure A.9: g85-s10, $D = 2.19mm, \sigma = 0.50$

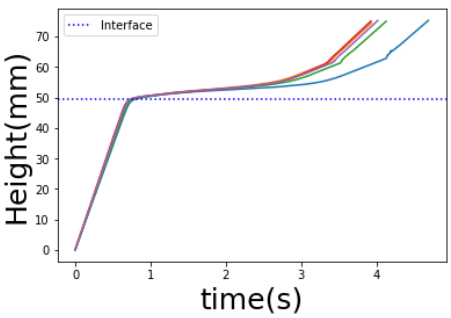

Figure A.10: g85-s350, $D = 4.45mm, \sigma = 0.12$

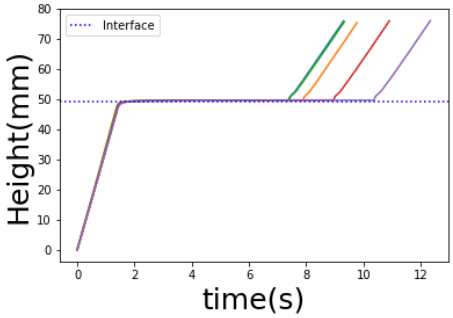

Figure A.11: g85-s350, $D = 2.77mm, \sigma = 0.18$

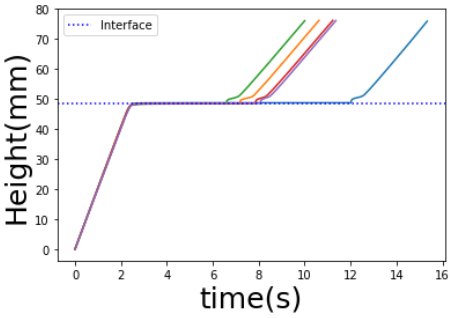

Figure A.12: g85-s350, $D = 2.19mm, \sigma = 0.35$

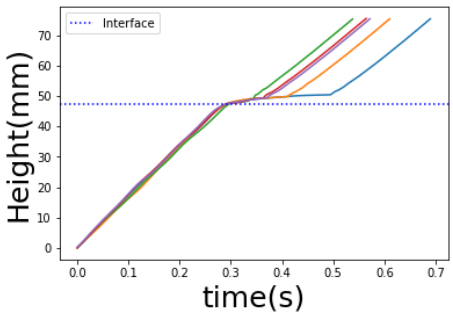

Figure A.13: w-s10, $D = 4.11mm, \sigma = 0.52$

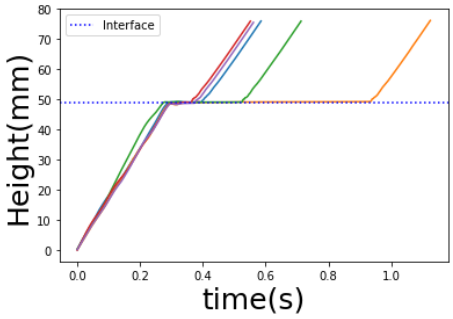

Figure A.14: w-s10, $D = 3.08mm, \sigma = 0.97$

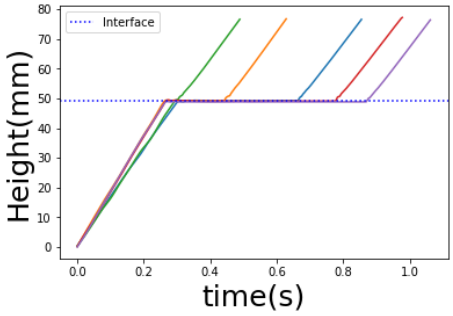

Figure A.15: w-s10, $D = 2.26mm, \sigma = 0.72$

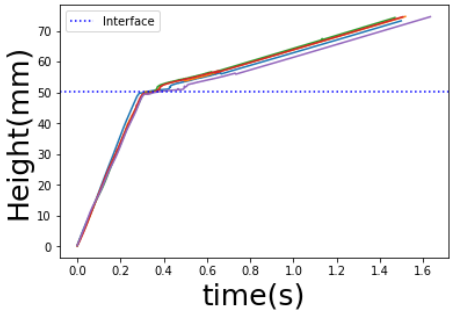

Figure A.16: w-s350, $D = 4.01mm, \sigma = 0.53$

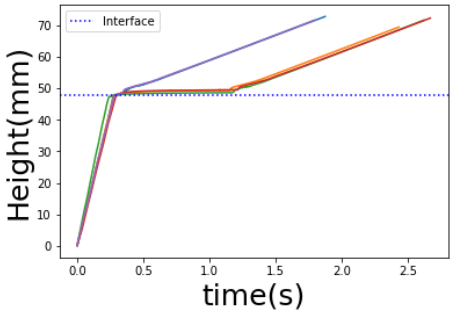

Figure A.17: w-s350, $D = 3.08mm, \sigma = 0.80$

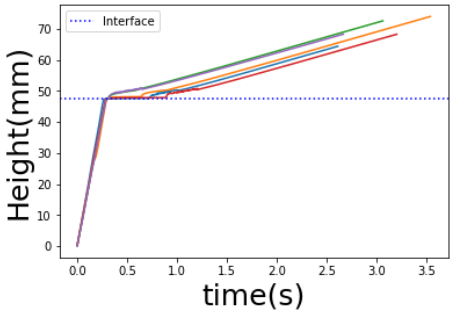

Figure A.18: w-s350, $D = 2.26mm, \sigma = 0.88$

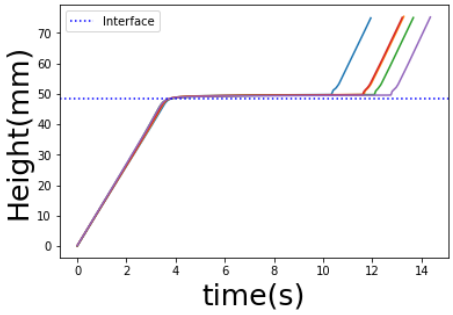

Figure A.19: g92-s350, $D = 3.46mm, \sigma = 0.11$

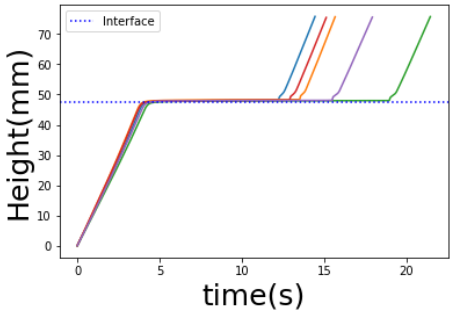

Figure A.20: g92-s350, $D = 2.75mm, \sigma = 0.24$

A.2 Tables

Table A.1: Complete table containing dimensionless numbers and retention times for all conducted experiments. The values in the table are the average of experimental sets of five.

multi phase system	$D_b(mm)$	Eö	$V_b(\frac{m}{s})$	Re_b	$\tau(s)$	$\frac{\mu_t}{\mu_b}$
water-sill10cSt	4.11	8.38	0.174	711	0.1196	9.6
water-sil10cSt	3.08	4.70	0.178	545	0.2176	9.6
water-sill10cSt	2.26	2.54	0.180	405	0.3344	9.6
water-sil 350cSt	4.01	11.32	0.177	706	0.0984	374
water-sil 350cSt	3.08	6.67	0.183	559	0.5760	374
water-sil 350cSt	2.26	3.61	0.170	384	0.2978	374
gly 53%-sil 10cSt	4.27	8.03	0.180	118	0.2532	1.30
gly 53%-sil 10cSt	2.82	3.50	0.164	71	0.5121	1.30
gly 53%-sil 10cSt	2.24	2.20	0.140	48	0.2815	1.30
gly 53%-sil 350cSt	4.35	8.86	0.182	122	0.9550	50.6
gly 53%-sil 350cSt	2.82	3.72	0.170	74	0.7283	50.6
gly 53%-sil 350cSt	2.24	2.34	0.142	49	0.3569	50.6
gly 85%-sil 10cSt	4.41	8.08	0.074	3.64	1.85	0.09
gly 85%-sil 10cSt	2.77	3.20	0.035	1.08	3.36	0.09
gly 85%-sil 10cSt	2.20	2.01	0.020	0.49	3.64	0.09
gly 85%-sil 350cSt	4.45	7.96	0.071	3.55	2.49	3.44
gly 85%-sil 350cSt	2.77	3.09	0.034	1.05	6.98	3.44
gly 85%-sil 350cSt	2.20	1.94	0.020	0.49	6.02	3.44
gly 92%-sil 350cSt	3.46	5.16	0.013	0.19	8.22	1.21
gly 92%-sil 350cSt	2.75	3.25	0.012	0.13	10.65	1.21

Table A.2: Complete table containing the dimensionles number of Weber and shape factors for all conducted experiments. The values in the table are the average of experimental sets of five.

multi phase system	$D_b(mm)$	We_b	$\frac{D_v}{D_h}_b$	We_t	$\frac{D_v}{D_h}_t$
water-sill10cSt	4.11	1.732	0.813	3.315	0.378
water-sil10cSt	3.08	1.360	0.864	2.952	0.471
water-sill10cSt	2.26	1.021	0.917	2.223	0.706
water-sil 350cSt	4.01	1.747	0.800	0.107	0.974
water-sil 350cSt	3.08	1.427	0.840	0.040	0.981
water-sil 350cSt	2.26	0.914	0.937	0.017	0.970
gly 53%-sil 10cSt	4.27	2.300	0.757	3.597	0.441
gly 53%-sil 10cSt	2.82	1.264	0.852	2.754	0.562
gly 53%-sil 10cSt	2.24	0.728	0.938	1.988	0.733
gly 53%-sil 350cSt	4.35	2.400	0.755	0.080	0.976
gly 53%-sil 350cSt	2.82	1.355	0.860	0.024	0.986
gly 53%-sil 350cSt	2.24	0.754	0.938	0.007	0.980
gly 85%-sil 10cSt	4.41	0.451	0.944	3.497	0.415
gly 85%-sil 10cSt	2.77	0.063	0.981	2.707	0.572
gly 85%-sil 10cSt	2.20	0.016	0.985	1.892	0.757
gly 85%-sil 350cSt	4.45	0.424	0.979	0.115	0.963
gly 85%-sil 350cSt	2.77	0.059	0.986	0.024	0.988
gly 85%-sil 350cSt	2.20	0.017	0.985	0.007	0.983
gly 92%-sil 350cSt	3.46	0.012	0.988	0.041	0.989
gly 92%-sil 350cSt	2.75	0.007	0.988	0.018	0.987

A.3 Experimental procedure

To obtain an experimental set, the following procedure is executed. An origin point is set on the column that is visible on both cameras in order to track a bubbles position across the cameras and as reference between different image sequences. The heavy liquid is added to the column to a predetermined height. Any air bubbles present in the heavy phase are removed. Before starting an experimental set, a lineal is put in the heavy phase of the column and an image is captured. With this image it is possible to obtain a pixel per mm ratio. A frequency test is performed in order to obtain the bubbles volume. The silicone oil light phase is added to the column, this is initially done slowly with a pipette in order to keep the interface as flat as possible. The bulk of light phase can then be added with a funnel. After running the MVP only the first bubble is captured with high speed imaging. The reason for this is because once a bubble passes the interface, the wet-ability of the interface gets disturbed. It is common that the first bubble elevates a part of the surface, which influences the passing conditions for consecutive bubbles. After one bubble is captured with high speed imaging the wet-ability of the interface gets restored by stirring the interface, this is done carefully since the purpose is only to restore the interface to its flat state, opposed to wetting the column walls with silicone oil. For each experimental set, a total of five bubbles are captured with high speed imaging. When an experimental set is done, only the top layer needs to be replaced for the next set. This is done by recovering most of the light phase with a pipette. The column is refilled with heavy phase. The refilled layer containing both heavy phase and light phase is removed and disposed in the low halogen organic waste bin. The top of the column is whipped with a paper. The new light phase can now be added. The first experimental set is performed with the lesser viscous silicone oil as the light phase, the consecutive experimental set is performed with the more viscous silicone oil.

A.4 Cleaning procedure

After a set of experiments with one bottom layer is completed, the column is cleaned. When cleaning the column it is of importance to remove as much silicone oil from the top as possible, initially before emptying the column. This is because the silicone oil can be reused and because the silicone oil has affinity for the walls, thus preventing the silicone oil to wet the bottom part of the column is convenient when cleaning. The light phase of silicone oil is recovered as much as possible with a pipette from the top of the column. The top of the column is then refilled with the heavy phase, this refilled layer containing both heavy phase and silicone oil is removed with a pipette and is disposed in the low halogen organic waste bin. The top of the column is whipped with a paper. The bottom phase is recovered by emptying the column. For rinsing the column options are limited, since liquids that dissolve the traces of silicone oil would harm the column. Therefore the column is rinsed with water and soap. The column is rinsed five times with hot water and soap, then the column is rinsed five times with demi-water. Let the column dry overnight or blow dry the column. The column can now be used for a new set of experiments.